International Journal of Nanomedicine

Dovepress
open access to scientific and medical research

Open Access Full Text Article

ORIGINAL RESEARCH

Poly(Acrylic Acid)-Modified MoS_2 Nanoparticle-Based Transdermal Delivery of Atenolol

This article was published in the following Dove Press journal:
International Journal of Nanomedicine

Kai Zhang[1]
Yanling Zhuang[2]
Jiwen Li[1]
Xiaochang Liu[3,4]
Shaoheng He[4]

[1]College of Science and Technology, Hebei Agricultural University, Cangzhou, People's Republic of China; [2]College of Humanities and Management, Hebei Agricultural University, Cangzhou, People's Republic of China; [3]School of Pharmacy, Shenyang Medical College, Shenyang, People's Republic of China; [4]Translational Medicine Research Centre, Shenyang Medical College, Shenyang, People's Republic of China

Introduction: Hypertension is a major health problem worldwide and is typically treated using oral drugs. However, the frequency of oral administration may result in poor patient compliance, and reduced bioavailability owing to the first-pass effect can also prove problematic.

Methods: In this study, we developed a new transdermal-drug-delivery system (TDDS) for the treatment of hypertension using atenolol (ATE) based on poly(acrylic acid) (PAA)-decorated three-dimensional (3D) flower-like MoS_2 nanoparticles (PAA-MoS_2 NPs) that respond to NIR laser irradiation. The PAA-modified MoS_2 NPs were synthesized and characterized using attenuated total reflection Fourier-transform infrared spectroscopy, X-ray diffraction measurements, scanning electron microscopy, transmission electron microscopy, dynamic light scattering, and the sedimentation equilibrium method. The drug-loading efficiency and photothermal conversion effect were also explored.

Results: The results showed that the colloidally stable PAA-MoS_2 NPs exhibited a high drug-loading capacity of 54.99% and high photothermal conversion ability. Further, the capacity of the PAA-MoS_2 NPs for controlled release was explored using in vitro drug-release and skin-penetration studies. The drug-release percentage was 44.72 ± 1.04%, and skin penetration was enhanced by a factor of 1.85 in the laser-stimulated group. Sustained and controlled release by the developed TDDS were observed with laser stimulation. Moreover, in vivo erythema index analysis verified that the PAA-MoS_2 NPs did not cause skin irritation.

Discussion: Our findings demonstrate that PAA-MoS_2 NPs can be used as a new carrier for transdermal drug delivery for the first time.

Keywords: transdermal drug delivery, poly(acrylic acid), atenolol, MoS_2 nanoparticles

Introduction

Hypertension, a risk factor for cardiovascular disease, stroke, renal disease, and several other disease processes, is a worldwide health problem.[1–3] Atenolol (ATE) is a β1-adrenergic receptor-blocking agent used to treat cardiovascular diseases and hypertension. Most commercially available atenolol preparations are oral immediate or extended-release formulations.[4] However, the frequency of administration may result in poor patient compliance, and oral administration can lead to reduced bioavailability owing to the first-pass effect.[5,6] An innovative drug-delivery system that avoids the first-pass effect and facilitates improved patient compliance is needed.

Correspondence: Xiaochang Liu
School of Pharmacy, Shenyang Medical College, Shenyang, People's Republic of China
Tel +86-24-62216610
Fax +86-24-62214089
Email liuxiaochang1991@163.com

submit your manuscript | www.dovepress.com
DovePress
http://doi.org/10.2147/IJN.S257906

Transdermal drug-delivery systems (TDDSs) are controlled release technologies that have attracted much interest in recent decades. TDDSs have many advantages, including avoiding the first-pass effect, improving patient compliance, reducing side effects, and increasing the duration of action, thereby decreasing dosing frequency.[6–9] With the development of materials science and nanotechnology, various nanomaterials have emerged as potential drug carriers for TDDSs.[10] In particular, inorganic nanomaterials, including Au- and Ag-based nanoparticles (NPs), have been studied extensively and have been widely used in TDDSs because of their high drug-loading capacity and good biocompatibility.[11] In addition, the two-dimensional nanomaterial graphene oxide has been used as a drug carrier for TDDS.[12,13] Materials used in TDDSs that are larger than 45 nm in size are stopped at the stratum corneum (SC) of untreated intact human skin and can therefore facilitate sustained and controlled release of drugs.[14]

MoS_2, a well-known type of two-dimensional transition metal dichalcogenide, has been used in various fields owing to its high specific surface area, easy surface modification, excellent photothermal conversion ability, and high absorbance in the near infrared (NIR) region.[15–18] Chou et al reported the biomedical application of chemically exfoliated MoS_2 (ce-MoS_2) as an NIR photothermal agent and showed that ce-MoS_2 exhibits greater photothermal performance relative to graphene and gold nanorods.[19] Because of its ultra-high specific surface area, MoS_2 has been employed as a drug carrier. Liu et al studiedpolyethylene glycol (PEG)-modified ce-MoS_2 and found that PEGylated ce-MoS_2 could be used as a carrier for the high-capacity loading of different drugs.[20] The loaded drug molecules can be controllably released upon photothermal induction by 808-nm NIR laser irradiation.[21] Haine et al investigated a gold nanorod-coated transparent polysaccharide hydrogel loaded with fluorescein isothiocyanate-modified ovalbumin as a TDDS for protein.[22] In addition, Teodorescu et al reported ondansetron-loaded Kapton/rGO patches as a novel TDDS.[23] These two studies demonstrated that laser irradiation can enhance the skin penetration of drugs or proteins. Thus, MoS_2 may have applications as a nanomaterial for the loading and delivery of drugs via TDDSs. However, the use of MoS_2 in a TDDS has not been reported previously.

Accordingly, in this study, we developed a new TDDS for the treatment of hypertension by ATE based on poly (acrylic acid) (PAA)-decorated three-dimensional (3D) flower-like MoS_2 NPs (PAA-MoS_2 NPs) that respond to 808-nm NIR laser irradiation.Our findings demonstrate, for the first time, that PAA-MoS_2 NPs can be used as a new carrier for transdermal drug delivery.

Materials and Methods

Materials

Ammonium molybdate tetrahydrate and thiourea were obtained from Shanghai Macklin Biochemical Co. Ltd. (Shanghai, China). Poly(acrylic acid) (PAA, Mw = 150,000 g/mol) was obtained from Shanghai Aladdin Bio-Chem Technology Co.Ltd. (Shanghai, China). Atenolol (ATE;HPLC, 98%) was purchased from Rhawn Chemical Technology Co. Ltd. (Shanghai, China). Methanol and phosphoric acid were of HPLC grade. Ultrapure water (18.2 MΩ) was used for all solution-based preparations. All other reagents were of analytical grade and used as received without any purification.

Synthesis of PAA-MoS_2 NPs

Flowerlike PAA-MoS_2 NPs were prepared via a one-step hydrothermal reaction (Figure 1). Ammonium molybdate tetrahydrate (1.24 g), thiourea (2.28 g), and PAA (1.24 g) were dissolved in ultrapure water (36 mL) under magnetic stirring. The mixture was stirred continuously for 30 min to form a homogeneous solution, before being transferred into a 50-mL Teflon-lined stainless-steel autoclave.It was heated at 220°C for 6 h and then naturally cooled down to room temperature. The black product was collected, washed with ultrapure water and ethanol several times, centrifuged at 11,000 rpm for 8 min to remove any impurities, and finally dried at 60°C under vacuum.

Characterisation of PAA-MoS_2 NPs

Attenuated total reflection Fourier-transform infrared (ATR-FTIR) spectra were recorded using a Perkin Elmer 2000 spectrophotometer with KBr pellets. X-ray diffraction (XRD) patterns were recorded using a Rigaku SmartLab X-Ray diffractometer with Cu Kα radiation. Scanning electron microscopy (SEM) images were acquired via a Hitachi SU8100 with an energy dispersive spectroscopy (EDS) unit. The latter was used to analyse elemental distributions. Transmission electron microscopy (TEM) and high-resolution TEM (HRTEM) images were acquired using a JEOL-2100F high-resolution TEM instrument. The colloidal stability was investigated using zeta potential measurements and the sedimentation equilibrium

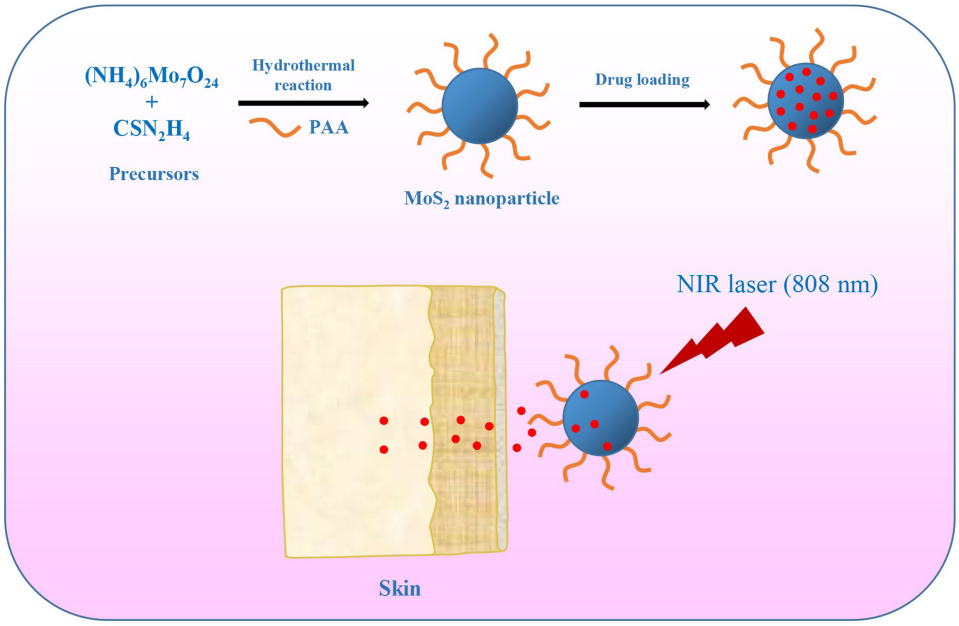

Figure 1 Schematic of PAA-MoS_2 NPs as a carrier capable of achieving the delivery of ATE and controlled drug release for transdermal administration.

method. The zeta potential was measured using dynamic light scattering (DLS, Melvin 2000). The sedimentation volume ratio was determined via the sedimentation equilibrium method, by recording the ratio of the heights after (H_u) and before (H_0) sedimentation.

Photothermal Conversion Performance

NIR laser irradiation (808 nm) produced by a multimode pump laser (F34-808ADX, Hashang Laser) was used to irradiate the PAA-MoS_2 NP solutions. Three concentrations (from 0.1 to 1.0 mg/mL) and three laser intensities were used to investigate the photothermal conversion performance. Further, the photothermal conversion stability was examined using three on-off cycles. The temperatures of the NP solutions were measured using the temperature-monitor attachment of the magnetic stirrer device.

Drug Loading

The drug-loading performance of the PAA-MoS_2 NPs toward was investigated in the bath mode. ATE solutions were prepared at different concentrations by dissolving various amounts of ATE in 100 mL of phosphate buffered saline (pH = 7.0). Then, 50 mg of PAA-MoS_2 NPs were added to the drug solution while stirring. Subsequently, the mixture was shaken with an oscillator at 32°C for 24 h. After achieving adsorption equilibrium, drug-loaded PAA-MoS_2 NPs (ATE-PAA-MoS_2) were obtained by centrifugation and the free drug concentrations in the samples were analysed by high-performance liquid chromatography with UV detection (HPLC-UV) to calculate the drug-loading efficiency. The latter was calculated as the ratio of the amounts of loaded drug and PAA-MoS_2 NPs.

In vitro Drug-Release Experiments

Two-chamber diffusion cells with an effective diffusion area of 1.5 cm^2 and a volume of 4.0 mL were used for the release study. A cellulose microporous membrane of 0.22 μm was caught between the two chambers. The donor solution was 0.5 mg/mL ATE-PAA-MoS_2 in water. The receptor cell was filled with phosphate buffered solution (PBS, pH 7.4) containing 15% PEG400. Samples of 2.0 mL from the receptor cell were withdrawn every hour for 8 h and replaced with accepter liquid of the same volume. Laser irradiation (1.0 W/cm^2, 5 min) was conducted after sampling at 1, 3, 5, and 7 h. The experiment was performed at 32 °C. The collected samples were analysed by HPLC-UV.

In vitro Skin Permeation Experiments

Male Wistar rats (180–220 g, 6–8 weeks old) were supplied by Liaoning Changsheng (Liaoning, China). Full-thickness skin was prepared by shaving the abdominal skin of the rats after they were anesthetized with urethane (20%, w/v; 6 mL/kg, i.p.). Then, the shaved skin was excised, and the adhering subcutaneous tissues were carefully removed. All procedures were performed in accordance with the NIH Guidelines for

the Care and Use of Laboratory Animals and were approved by the Animal Ethics Committee of Shenyang Medical College.

The prepared skin was fixed between two cells with the stratum corneum facing the donor solution. All the procedures for the skin-penetration experiments were similar to those for the drug-release study, except for the fact that the samples were collected at 2, 4, 6, and 8h, and the donor solution was irradiated after each sampling event. The collected samples were analyzed using HPLC-UV.

HPLC-UV Analysis of the Drug

Samples were analysed using an HPLC system (Tokyo, Japan) consisting of an L-2420 ultraviolet-absorbance detector and L-2130 pump. An ODS2 C18 reverse-phase stainless-steel column (200×4.6 mm, 5 μm; Waters, America) was used for the separation and the column temperature was maintained at 25 °C. The mobile phase was composed of methanol, water, and phosphoric acid solution (70:30:0.1, v/v) and the flow rate was 0.7 mL/min. The detection wavelength was set to 275 nm.

In vivo Skin Erythema Study

The erythema index (EI) of the skin was measured by using a Mexameter® instrument (MX 16, Courage &Khazaka Co., Germany) to evaluate the biocompatibility of the PAA-MoS_2 NPs. Rabbits were used to assess the potential skin irritation caused by PAA-MoS_2 NPs, with a 10% (w/v) sodium dodecyl sulfate (SDS) water solution as the positive control. The dorsal skin of the rabbits was shaved and divided into four separate sections, each with an area of 2.5 × 2.5 cm. To obtain a baseline EI value (EI_0), the EI values of the sections were measured before the topical application of the irritants. PBS (500 μL) PAA-MoS_2 NPs (without laser irradiation), PAA-MoS_2 NPs (with 5-min laser irradiation),or 10% SDS was dropped onto the respective sections. After 8 h, the excess solution was removed, and the sections were cleaned with cotton wool swabs, with laser irradiation being performed before the solution was removed for the relevant samples. EI_t values were measured and ΔEI values were calculated by subtracting EI_0 from EI_t. This experiment was quadruplicated.

Statistical Analysis

All numerical results obtained are expressed as mean ± S. D. The data were subjected to an analysis of variance (ANOVA), using SPSS 16.0 software. The level of significance was taken as $p< 0.05$.

Results

Characterisation of PAA-MoS_2 NPs

Flower-like PAA-MoS_2 NPs were synthesized via a one-pot method and further characterized by ATR-FTIR, XRD, SEM, and HRTEM. ATR-FTIR spectroscopic analysis was used in this study to evaluate the surface modification of MoS_2 by PAA. The IR spectrum of PAA, MoS_2 and PAA-MoS_2 NPs are presented in Figure 2. The peak at 1711 cm^{-1} is a characteristic IR band of C=O in PAA, which was clearly observed in the spectra of PAA-MoS_2 NPs. There was no significant change on the wavenumber of PAA, indicating it was possible that PAA simply inserted in the crystal of MoS_2. Overall, these results indicate that PAA is successfully bound to the surface of MoS_2.

The XRD patterns of PAA and flower-like PAA-MoS_2 NPs are shown in Figure 3A and B respectively. The peaks at 2θ = 14.4°, 32.7°, 39.5°, 49.8°, and 58.3° correspond to the (002), (100), (103), (105), and (110) planes of hexagonal MoS_2 (JCPDS card no. 37–1492) (Figure 3B).[24] No other diffraction peaks appear in the patterns. The diffraction peak at 14.4°is sharper and narrower, indicating that a well-ordered, layered MoS_2 structure was successfully synthesised. This is consistent with the data for pure MoS_2 reported in the literature.[25] Moreover, the peaks of PAA is not observed in the Figure 3B, indicating that PAA was uniformly distributed in MoS_2.

SEM images of PAA-MoS_2 NPs are shown in Figure 4A and B. The images depict several uniform flower-like PAA-MoS_2 NPs having a mean diameter of approximately 500 nm. Figure 4B shows a clear view of the surface morphology, indicating that the formation of the flower-like PAA-MoS_2 NPs occurs via self-assembly and by the crimping of nanosheets. The TEM image (Figure 4C) shows typical flower-like PAA-MoS_2 NPs. The HRTEM image (Figure 4D) reveals more detailed structural information on the PAA-MoS_2 samples. These results demonstrate that the samples were formed by the overlapping and curling of many molybdenum disulfide nanosheets, consistent with our SEM results. Moreover, the lattice spacing of the (002) plane of the flower-like PAA-MoS_2 NPs is 0.63 nm, consistent with the abovementioned XRD results. Furthermore, elemental mapping shows that the elements are well dispersed across the surface of the sample (Figure 5).

Zeta potential and sedimentation volume ratio measurements were introduced to explore the colloidal stability of the NPs. The zeta potential of the MoS_2 NPs was

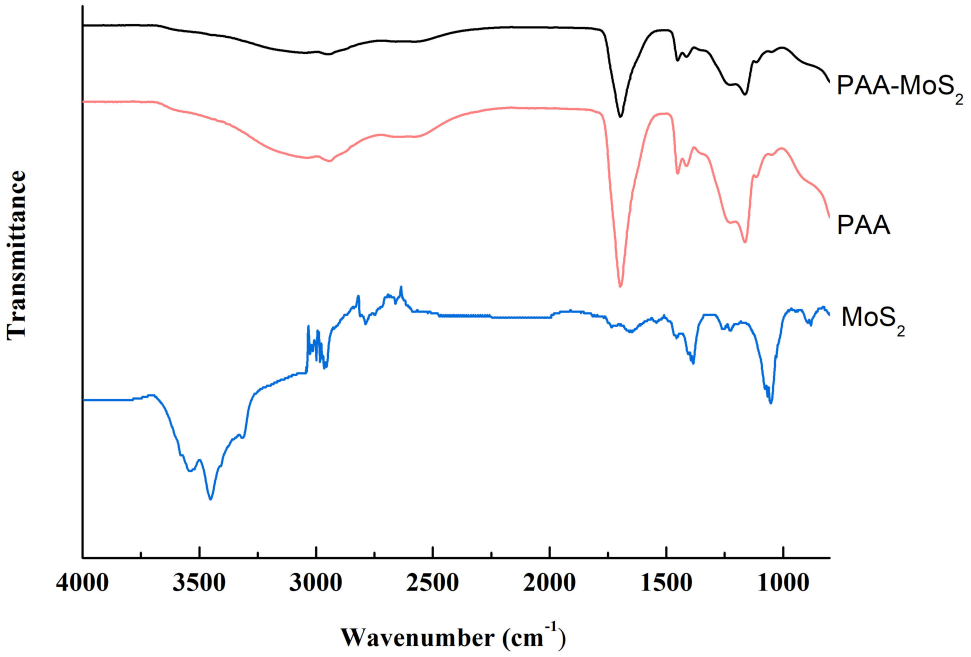

Figure 2 ATR-FTIR spectra of PAA-MoS_2 NPs.

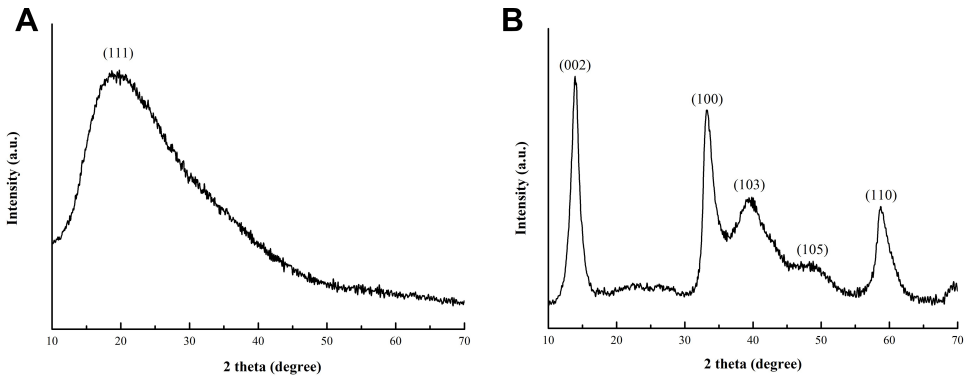

Figure 3 XRD pattern for the as-prepared PAA **(A)** and PAA-MoS2 NPs **(B)**.

measured to be −14.64 ±1.72 mV, while that of the PAA-MoS_2 NPs was significantly increased (−27.49 ± 3.24 mV). Moreover, after 5 days of sedimentation, H_u/H_0 values for the PAA-MoS_2 NPs and MoS_2 NPs were 0.87 ± 0.06 and 0.22 ± 0.12, respectively. These results indicate that PAA fictionalization increased the stability of the nanoparticles.

Photothermal Conversion Performance Study

The photothermal conversion abilities of PAA-MoS_2 NPs and water were determined,with and without laser stimulation (Figure 6). Our results show that water exhibits no photothermal conversion ability, even under intense laser irradiation (1.0 W/cm^2). However, temperatures up to 89.2°C were obtained for the PAA-MoS_2 NP solution within 5 min of irradiation (0.5 W/cm^2, 1.0 mg/mL). A laser intensity of 0.5 W/cm^2 and NP concentration of 0.5 mg/mL, considering photodamage, were selected as the optimal values for these parameters. Moreover, the stability of the photothermal conversion was confirmed by measurements over three on-off cycles (Figure 6C). These results indicate that the photothermal conversion ability was not affected by PAA modification.

Drug-Loading Efficiency

The drug-loading efficiency of PAA-MoS_2 NPs with respect to ATE was evaluated by determining the concentration of

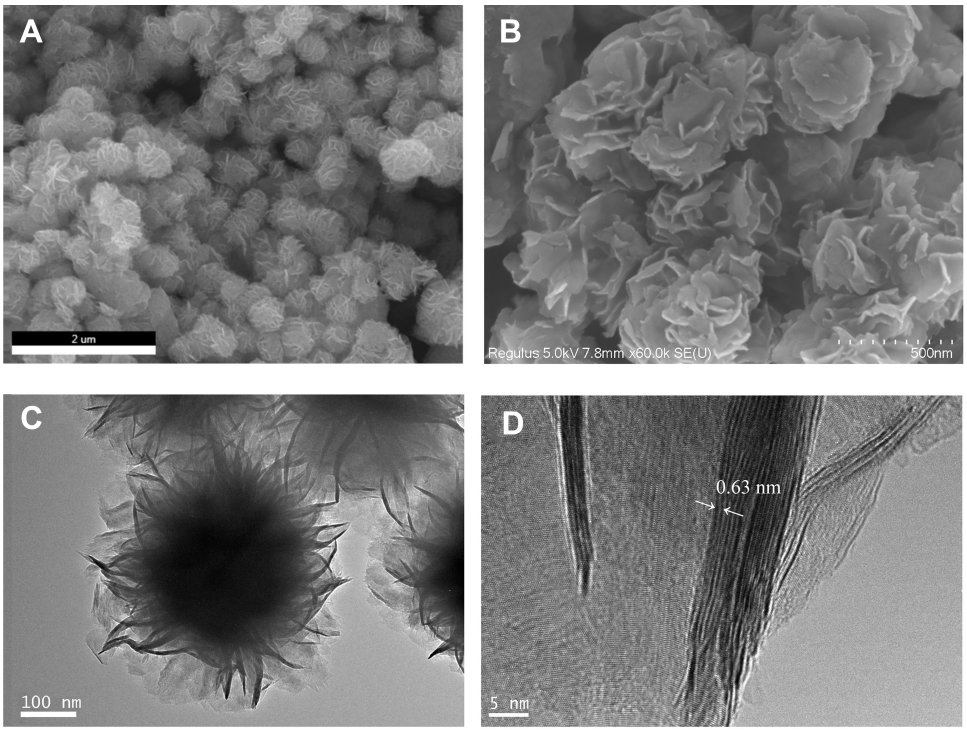

Figure 4 SEM (**A** and **B**) and TEM (**C** and **D**) of the PAA-MoS_2 NPs.

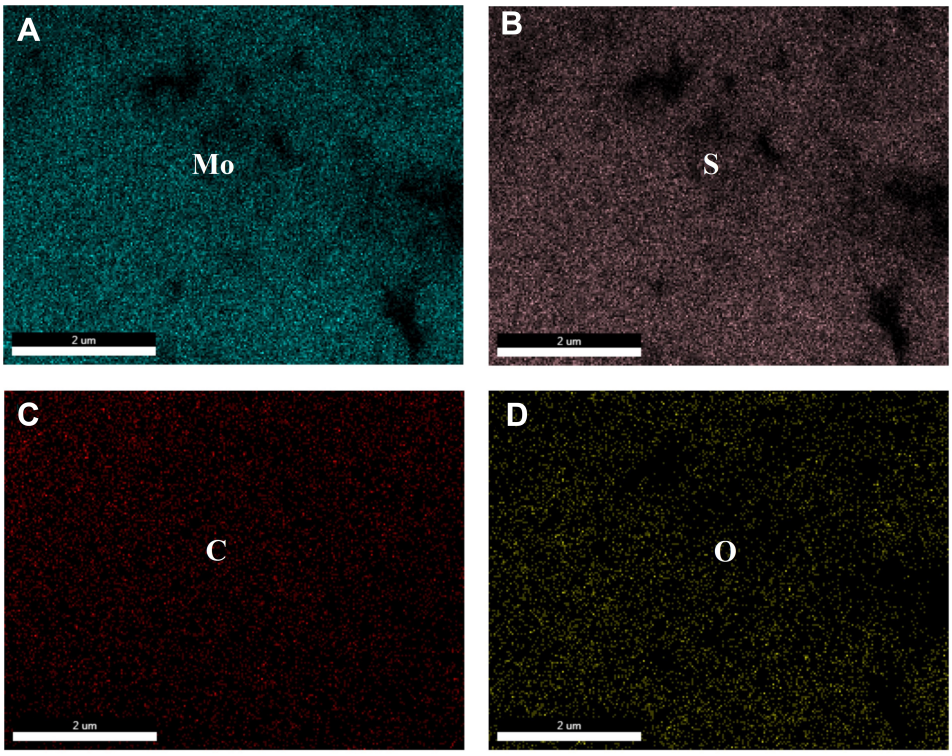

Figure 5 Elemental mapping images of PAA-MoS2 composites: **(A)** Mo element, **(B)** S element, **(C)** C element and **(D)** O element.

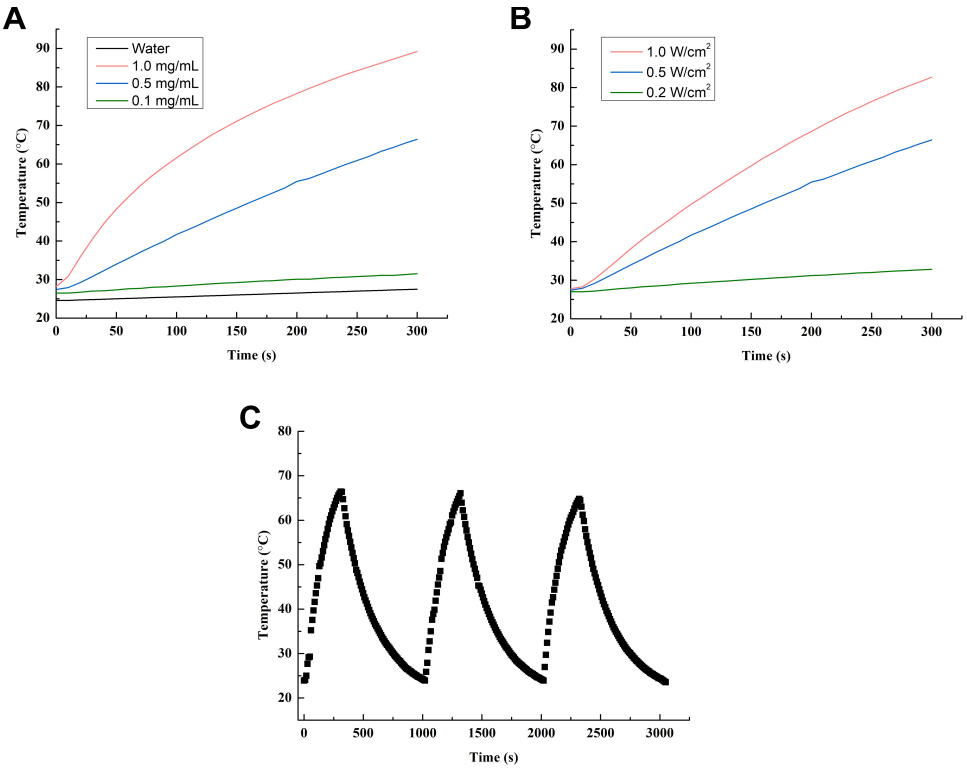

Figure 6 Heating curves of (**A**) various PAA-MoS_2 NPs concentrations under a laser power of 0.5 W/cm^{-2}, (**B**) PAA-MoS_2 NPs of 0.5 mg/mL under varying laser powers, and (**C**) PAA-MoS_2 NPs over three on-off cycles (0.5 W/cm^2, 0.5 mg/mL).

free ATE in the solution before and after loading using HPLC-UV methods. Concentrations greater than the solubility of ATE were not investigated in this study, to avoid waste. As shown in Figure 7, the ATE-loading efficiency increases with the ATE concentration. A PAA-MoS_2 NP concentration of 0.5 mg/mL and an ATE concentration of 2.0 mg/mL were obtained as optimized values from subsequent experiments. As a result, a loading efficiency of 54.99± 0.66% was achieved when the ATE/PAA-MoS_2 NP ratio was 4 (pH=7), signifying that 1 g of PAA-MoS_2 NPs could be loaded with 0.55 g of ATE.

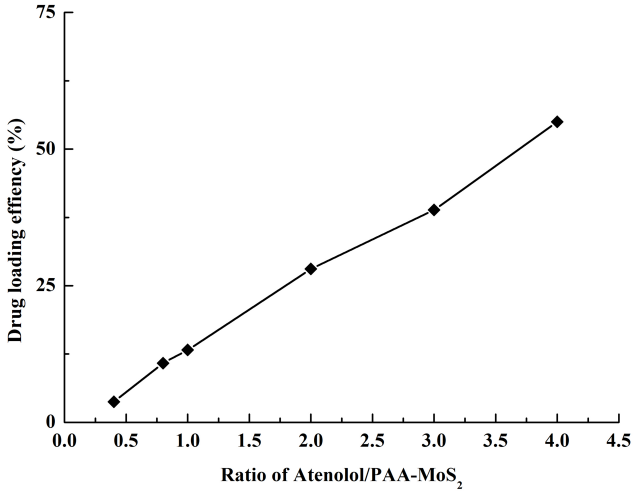

Figure 7 Drug loading efficiency achieved at various mass ratios of ATE to PAA-MoS_2 NPs.

Drug-Release and Skin-Penetration Analyses

The results of the in vitro drug-release tests are shown in Figure 8A. The drug-release percentage in the laser-stimulated group is 44.72 ± 1.04%, which is 1.5-fold higher than that of the control group. Moreover, an increase is observed at every time point after light stimulation,and greater sustained release was observed in the laser-stimulation group. These results indicate that light stimulation is an effective method to control the release of ATE from PAA-MoS_2 NPs.

The enhancing effect of laser stimulation on PAA-MoS_2 NPs was further demonstrated via in vitro skin-penetration experiments. As shown in Figure 8B, in contrast to the control group, a slight but significant enhancement of the percutaneous absorption of ATE, yielding an enhancement ratio of 1.85 (p<0.05), is observed in the laser stimulation group. In addition, drug penetration is significantly enhanced

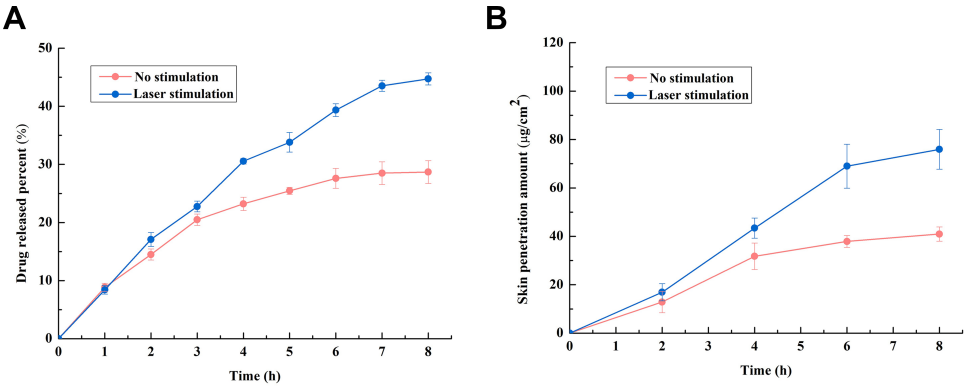

Figure 8 **(A)** Drug release with and without laser stimulation, **(B)** skin penetration of ATE released from PAA-MoS_2 NPs with and without laser stimulation.

immediately after laser stimulation, which could be meaningful for eliciting therapeutic effects.

In vivo Skin Erythema Study

A non-invasive in vivo skin erythema measurement was used to monitor irritation caused by the PAA-MoS_2 NPs. As shown in Figure 9, ΔEI increases significantly after the topical application of 10% SDS, indicating that the rabbits respond normally to this skin irritant. Application of the PAA-MoS_2 NPs suspended in water does not increase ΔEI, indicating the high biocompatibility of the PAA-MoS_2 NPs. Furthermore, laser stimulation of the PAA-MoS_2 NPs temporarily increases the erythema index, but this skin irritation is reversible.

Discussion

Polymer-bound inorganic nanomaterials have become a research hotspot in the field of drug delivery. Compared with inorganic nanomaterials, polymers have greater structural adjustability and can be designed as drug carriers to meet clinical requirements.[26] By controlling the hydrophilic and hydrophobic balance, and by introducing functional groups and drugs, different types of administration can be tailored, including nanoparticles, injectable hydrogels, and coatings. In this work, PAA molecules were chosen as modifiers because they are biocompatible, hydrophilic polymers that are widely used in the biomedical field.[27–29] We established a simple PAA-mediated one-pot synthesis of MoS_2 NPs with simultaneous surface modification. The structure, grain size, morphology, and stability of the prepared PAA-MoS_2 NPs were thoroughly investigated via ATR-FTIR, XRD, SEM, HRTEM, DLS, and sedimentation equilibrium experiments. Based on our analysis of the above characterisation results and related literature,[25,30] we were able to demonstrate that PAA was successfully modified on the surface of MoS_2 without destruction of the basic crystal structure of MoS_2.

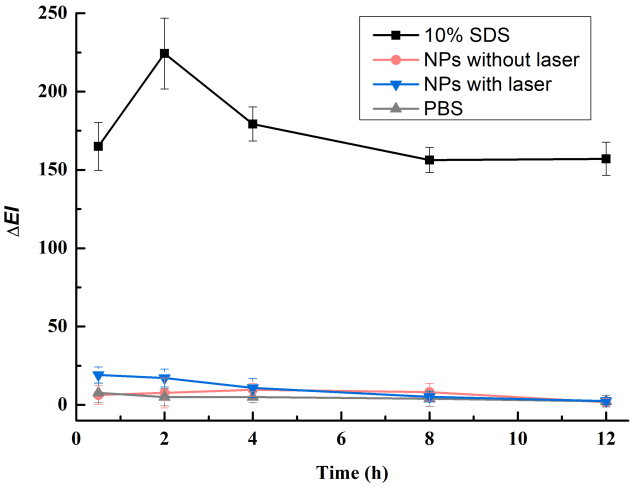

Figure 9 Skin penetration of ATE released from PAA-MoS_2 NPs with and without NIR stimulation.

The presence of the hydrogen bond receptor C=O and hydrogen bond donor OH in carboxyl groups of PAA made it a good choice for drug delivery. PAA functionalization increased the colloidal stability of the MoS_2 nanoparticles, which was in agreement with the results of Molnar et al.[27] The probable cause of this stability enhancement was the fact that the carboxyl groups in PAA increased the number of interactions between the PAA-MoS_2 NPs and water molecules. Furthermore, the PAA modification increased the drug-loading capacity of the MoS_2 NPs. Compared with a previous study in which polyvinylpyrrolidone was used to modify the surfaces of MoS_2 NPs,[17] the PAA-MoS_2 NPs exhibited higher drug loading amounts, with 1 g of PAA-MoS_2 NPs supporting a load of 0.55 g of ATE. Kim et al[31] demonstrated that COOH groups in acrylic adhesives formed strong ionic

interactions with NH_2groups in tacrine, which increased the interaction energy between the drug and the adhesives. Besides the large surface area of porous 3D flower-like MoS_2 NPs, the COOH groups of PAA also provided a site for binding ATE, which includes an NH_2 group. The conjugation of atenolol molecules onto PAA-MoS2 was achieved probably by hydrophobic interactions, hydrogen bonds and ionic interaction.[6,20] Moreover, Liu et al demonstrated that carboxyl-containing excipients provided a strong controlling force for basic drugs, which is an important factor for extended preparations.[6] Hu et al found that the inclusion of PAA in chitosan-PAA complexed nanoparticles significantly influenced the release of silk peptide.[28] It is possible, therefore, that PAA might also control drug release in the preparation.

In addition to drug-excipient interactions, NIR laser stimulation,a method often used to control drug release from nano platforms,[32] proved to be another important factor influencing drug release in this TDDS. The photothermal effects of inorganic nanomaterials are a promising property for drug release. The photothermal conversion effect of PAA-MoS_2 NPs was also investigated in this study. We used a wavelength of 808 nm, which is commonly used to stimulate MoS_2 NPs. The use of this NIR wavelength avoids photodamage to the skin,[17] as confirmed by the results of the in vivo erythema index experiments. As the results in Figure 9 show, laser stimulation significantly increases the release of ATE and prolongs the permeation of the skin by ATE. Drug transdermal penetration involves two important steps, drug release from the preparation and percutaneous absorption, which are generally considered to be passive diffusion processes.[33] The diffusion of both drug molecules and intercellular lipids in stratum corneum could be enhanced by increasing the temperature of the skin.[34] Thus, the photothermal conversion ability of PAA-MoS_2 NPs not only enhanced drug release but also promoted ATE permeation through the skin.

Conclusion

In summary, in this study, we reported the synthesis of colloidally stable PAA-MoS_2 NPs to transdermal delivery ofATE for the treatment of hypertension for the first time. Owing to the ultra-high specific surface area and special structure of PAA, PAA-MoS_2 NPs underwent reasonably efficient ATE binding. NIR laser stimulation successfully enhanced drug release and transdermal drug permeation from PAA-MoS_2 NPs. This study was a primary exploration of the transdermal application of PAA-MoS_2 NPs. Further studies are required for formulation optimization and in vivo confirmation of the loaded ATE-PAA-MoS_2 composite as a TDDS before clinical application.

Acknowledgments

This work has been supported by Specialized Research Fund for Introducing Talents of Hebei Agricultural University (No. YJ201908), Shenyang Medical College of Science and Technology Fund Project (No. 20186073) and Liaoning Science and Technology (No. 20180550409).

Disclosure

The authors report no conflicts of interest in this work.

References

1. Mills KT, Bundy JD, Kelly TN, et al. Global disparities of hypertension prevalence and control. *Circulation*. 2016;134:441–450. doi:10.1161/CIRCULATIONAHA.115.018912
2. Vavricka SR, Himmelmann A, Schaffner A. Age-specific relevance of usual blood pressure to vascular mortality: a meta-analysis of individual data for one million adults in 61 prospective studies. *Lancet*. 2002;360:1903–1913.
3. Vasan RS, Larson MG, Leip EP, et al. Impact of high-normal blood pressure on the risk of cardiovascular disease. *N Engl J Med*. 2001;345:1291–1297. doi:10.1056/NEJMoa003417
4. Maboos M, Yousuf RI, Shoaib MH, et al. Effect of lipid and cellulose based matrix former on the release of highly soluble drug from extruded/spheronized, sintered and compacted pellets. *Lipids Health Dis*. 2018;17:136. doi:10.1186/s12944-018-0783-8
5. Ahad A, Al-Jenoobi FI, Al-Mohizea AM, et al. Systemic delivery of β-blockers via transdermal route for hypertension. *Saudi Pharm J*. 2014;23:587–602. doi:10.1016/j.jsps.2013.12.019
6. Liu C, Quan P, Li S, et al. A systemic evaluation of drug in acrylic pressure sensitive adhesive patch, in vitro, and, in vivo: the roles of intermolecular interaction and adhesive mobility variation in drug controlled release. *J Control Release*. 2017;252:83–94. doi:10.1016/j.jconrel.2017.03.003
7. Alexander A, Dwivedi S, Giri TK, Saraf S, Saraf S, Tripathi DK. Approaches for breaking the barriers of drug permeation through transdermal drug delivery. *J Control Release*. 2012;164(1):26–40. doi:10.1016/j.jconrel.2012.09.017
8. Ahad A, Aqil M, Ali A. Investigation of antihypertensive activity of carbopol valsartan transdermal gel containing 1,8-cineole. *Int J Biol Macromol*. 2014;64:144–149. doi:10.1016/j.ijbiomac.2013.11.018
9. Ahad A, Aqil M, Kohli K, et al. Chemical penetration enhancers: a patent review. *Expert Opin Ther Pat*. 2009;19(7):969–988. doi:10.1517/13543770902989983
10. Zhou X, Hao Y, Yuan L, et al. Nano-formulations for transdermal drug delivery: a review. *Chin Chem Lett*. 2018;29:1713–1724. doi:10.1016/j.cclet.2018.10.037
11. Alba-Molina D, Giner-Casares JJ, Cano M. Bioconjugated plasmonic nanoparticles for enhanced skin penetration. *Top Curr Chem*. 2019.378(1):8.
12. Kurniawan A, Muneekaew S, Hung C-W, et al. Modulated transdermal delivery of nonsteroidal anti-inflammatory drug by macroporous poly(vinyl alcohol)-graphene oxide nanocomposite films. *Int J Pharm*. 2019;566:708–716. doi:10.1016/j.ijpharm.2019.06.029

13. Chen Y, Yang Y, Xian Y, et al. Multifunctional graphene-oxide-reinforced dissolvable polymeric microneedles for transdermal drug delivery. *ACS Appl Mater Interfaces*. 2020;12(1):352–360. doi:10.1021/acsami.9b19518
14. Labouta HI, el-Khordagui LK, Kraus T, et al. Mechanism and determinants of nanoparticle penetration through human skin. *Nanoscale*. 2011;3:4989–4999. doi:10.1039/c1nr11109d
15. Liu J, Zheng J, Nie H, et al. Co-delivery of erlotinib and doxorubicin by MoS_2 nanosheets for synergetic photothermal chemotherapy of cancer. *Chem Eng J*. 2019. 381:122541.
16. Dong X, Yin W, Zhang X, et al. Intelligent MoS_2 nanotheranostic for targeted and enzyme-/pH-/NIR-responsive drug delivery to overcome cancer chemotherapy resistance guided by PET imaging. *ACS Appl Mater Interfaces*. 2018;10:4271–4284. doi:10.1021/acsami.7b17506
17. Yang H, Zhao J, Wu C, et al. Facile synthesis of colloidal stable MoS_2 nanoparticles for combined tumor therapy. *Chem Eng J*. 2018;351:548–558. doi:10.1016/j.cej.2018.06.100
18. Sun Y, Wu X, Zhang K, et al. Electrochemiluminescent quaternary Cu-Zn-In-S nanocrystals as a sensing platform: enzyme-free and sensitive detection of the FLT3 gene based on triple signal amplification. *BiosensBioelectron*. 2018;100:445–452. doi:10.1016/j.bios.2017.09.026
19. Chou SS, Kaehr B, Kim J, et al. Chemically exfoliated MoS_2 as near-infrared photothermal agents. *Angew Chem Int Ed*. 2013;52:1–6. doi:10.1002/anie.201209229
20. Liu T, Wang C, Gu X, et al. Drug delivery with PEGylated MoS_2 nano-sheets for combined photothermal and chemotherapy of cancer. *Adv Mater*. 2014;26:3433–3440. doi:10.1002/adma.201305256
21. Yin W, Yan L, Yu J, et al. High-throughput synthesis of single-layer MoS_2, nanosheets as a near-infrared photothermal-triggered drug delivery for effective cancer therapy. *ACS Nano*. 2014;8:6922–6933. doi:10.1021/nn501647j
22. Haine AT, Koga Y, Hashimoto Y, et al. Enhancement of transdermal protein delivery by photothermal effect of gold nanorods coated on polysaccharide-based hydrogel. *Eur J Pharm Biopharm*. 2017;119:91–95. doi:10.1016/j.ejpb.2017.06.005
23. Teodorescu F, Gurvan Q, Foulon C, et al. Transdermal skin patch based on reduced graphene oxide: a new approach for photothermal triggered permeation of ondansetron across porcine skin. *J Control Release*. 2017;245:137–146. doi:10.1016/j.jconrel.2016.11.029
24. Ahmad H, Aidit SN, Ooi SI, et al. Tunable passively Q-switched erbium-doped fiber laser with Chitosan/MoS_2</sub> saturable absorber. *Opt Laser Technol*. 2018;103:199–205. doi:10.1016/j.optlastec.2018.01.032
25. Tang G, Wang Y, Chen W, et al. Hydrothermal synthesis and characterization of novel flowerlike MoS_2 hollow microspheres. *Mater Lett*. 2013;100:15–18. doi:10.1016/j.matlet.2013.02.103
26. Liang R, Wei M, Evans DG, et al. Inorganic nanomaterials for bioimaging, targeted drug delivery and therapeutics. *Chem Commun*. 2014;50:14071–14081. doi:10.1039/C4CC03118K
27. Molnar RM, Bodnar M, Hartmann JF, et al. Preparation and characterization of poly(acrylic acid)-based nanoparticles. *Colloid Polym Sci*. 2009;287:739–744. doi:10.1007/s00396-009-2033-0
28. Hu Y, Jiang X, Ding Y, et al. Synthesis and characterization of chitosan-poly(acrylic acid) nanoparticles. *Biomaterials*. 2002;23:3193–3201. doi:10.1016/S0142-9612(02)00071-6
29. Liang S, Liu Y, Fu T, et al. A water-soluble and biocompatible polymeric nanolabel based on naphthalimide grafted poly(acrylic acid) for the two-photon fluorescence imaging of living cells and C. elegans. *Colloid Surf B*. 2016;148:293–298. doi:10.1016/j.colsurfb.2016.09.001
30. Zhang X, Huang X, Xue M, et al. Hydrothermal synthesis and characterization of 3D flower-like MoS_2 microspheres. *Mater Lett*. 2015;148:67–70. doi:10.1016/j.matlet.2015.02.027
31. Kim JH, Cho YJ, Choi HK. Effect of vehicles and pressure sensitive adhesives on the permeation of tacrine across hairless mouse skin. *Int J Pharm*. 2000;196:105–113. doi:10.1016/S0378-5173(99)00449-4
32. Choi M, Kim KG, Heo J, et al. Multilayered graphene nano-film for controlled protein delivery by desired electro-stimuli. *Sci Rep*. 2015;5:17631. doi:10.1038/srep17631
33. Song W, Quan P, Li S, et al. Probing the role of chemical enhancers in facilitating drug release from patches: mechanistic insights based on FT-IR spectroscopy, molecular modeling and thermal analysis. *J Control Release*. 2016;227:13–22. doi:10.1016/j.jconrel.2016.02.027
34. Liu X, Quan P, Li S, et al. Time dependence of the enhancement effect of chemical enhancers: molecular mechanisms of enhancing kinetics. *J Control Release*. 2017;248:33–44. doi:10.1016/j.jconrel.2017.01.017